iSoft: A Customizable Soft Sensor with Real-time Continuous Contact and Stretching Sensing

Sang Ho Yoon, Ke Huo, Yunbo Zhang, Guiming Chen, Luis Paredes, Subramanian Chidambaram, Karthik Ramani

School of Mechanical Engineering, Purdue University, West Lafayette, IN, USA
{yoon87, khuo, zhan2014, chen1956, lparede, schidamb, ramani}@purdue.edu

ABSTRACT

We present *iSoft*, a single volume soft sensor capable of sensing real-time continuous contact and unidirectional stretching. We propose a low-cost and an easy way to fabricate such piezoresistive elastomer-based soft sensors for instant interactions. We employ an electrical impedance tomography (EIT) technique to estimate changes of resistance distribution on the sensor caused by fingertip contact. To compensate for the rebound elasticity of the elastomer and achieve real-time continuous contact sensing, we apply a dynamic baseline update for EIT. The baseline updates are triggered by fingertip contact and movement detections. Further, we support unidirectional stretching sensing using a model-based approach which works separately with continuous contact sensing. We also provide a software toolkit for users to design and deploy personalized interfaces with customized sensors. Through a series of experiments and evaluations, we validate the performance of contact and stretching sensing. Through example applications, we show the variety of examples enabled by *iSoft*.

ACM Classification Keywords

H.5.2. [Information Interfaces and Presentation]: User Interfaces. − Input devices and strategies

Author Keywords

Wearables; Soft Sensor; Sensing Technique; Input Device; Customization

INTRODUCTION

Stretchable soft sensors have been explored as promising input methods for adding interactions on both rigid and elastic physical objects, smart textiles, shape-changing surfaces, humanoids, and the human body [22, 30, 32, 50, 51]. With a high flexibility and stretchability of the sensors, a wide scope of natural interactions such as contacting [43], bending [4], squeezing [47], and stretching [44] have been suggested. Still, the expensive and multi-step fabrication processes keep people from quickly making and deploying inexpensive, customized soft sensors.

Recent approaches have shown the potential for reducing the fabrication complexity [51] and improving the design freedom [50] for soft-matter sensors. These previous works focused on employing capacitive sensing and demonstrated discrete inputs such as touching and pressing. To support more advanced inputs such as contact localization and continuous tracking, a common solution for capacitive sensing is via a sensing array which further introduces complexities in both design and fabrication. Moreover, developing multi-modal sensing capability through capacitive sensing by using a single-volume sensor could be difficult. Further, ad-hoc modifications on the prototyped sensor shapes and ease of deploying the sensors show significant opportunity for creating customized interfaces [6, 28]. Yet instantiations of such paradigms have not been fully studied for soft sensors. By emphasizing these directions, we investigate a *single-volume soft-matter* sensor that provides *multimodal sensing*. Our approach allows users to fabricate sensors inexpensively, customize interfaces easily, and deploy them instantly.

We take advantage of carbon-filled liquid silicone rubber, a non-toxic piezoresistive material which has been widely explored for different types of low-cost, easy-to-implement sensing methods [49]. The major hurdle in employing the carbon-filled silicone as an interaction input is the lack of real-time sensing capability. This is mainly due to a rebound elasticity of the material, which causes a slow-recovery of the sensing signals after material deformations. In a previous work, a modeling approach was proposed [25] for posture estimation, but a solution for real-time continuous contact localization has not been fully studied. In our work, we adopt a dynamic baseline update process using the EIT approach to achieve real-time continuous contact localization. In addition, the carbon elastomer has been used for building a single-layer wearable sensor which supports multiple sensing modalities such as finger pressing and bending [55]. Here, we also utilize stretching which enables multimodal sensing with *iSoft*.

By employing the EIT technique, we can interface the sensor by placing electrodes on the sensor boundary only. In this way, the sensor can be fabricated in a single-volume manner and implemented without invasive wirings. Recent work with EIT sensing has shown its potential for touch sensing on an arbitrary surface using machine learning models [57]. We extend the EIT sensing to the soft-matter sensors with multimodal sensing capability. Moreover, we propose a customization toolkit for users to support the design and deployment of the

sensors. To this end, we allow users to perform interactions instantly after deployment without any extra training processes.

In this work, we introduce *iSoft*, which supports multimodal inputs based on the deformation of a single-volume carbon-filled elastomer. Our prototype supports real-time continuous contact and stretching sensing. Using the proposed fabrication method, a sensing technique, and a software toolkit, we entitle users with the ability to create and customize soft-matter sensors even if they have no professional knowledge on material processing and use of specialized processing equipment. Our contributions are as follows:

- A novel sensing technique providing real-time continuous contact and stretching sensing with carbon-filled elastomer;

- Hardware and software workflows that enable users to customize and deploy soft sensors for instant interactions; and

- Example applications demonstrating the use of the multimodal sensing capability of the proposed soft sensors.

RELATED WORK

Soft Sensors & Sensing Modality
Recent developments in soft sensors have shown their capability for complex sensing with high flexibility and stretchability [5]. With the advancements in materials, the soft sensors have enabled the measurement of highly accurate contact pressure, strain, and shear deformations [24, 30, 37]. However, the fabrication of these sensors still requires expensive materials and complex fabrication treatments. To this extent, recent works in HCI have demonstrated fabricating soft sensors for adding touch interactions to physical objects and human body [50, 51]. Our work also maintains the spirit of low-cost soft-matter sensors by introducing a simple fabrication process along with a customization software toolkit.

Different forms of sensing have been explored for soft sensors to promote natural motions and behaviors as an input. Previous works have been fundamentally based on sensing the mechanical strain and introduced various sensing modalities such as contact pressure [8, 27, 35], bending [4, 36, 43], and stretching [14, 44] for input interfaces. Along these directions, a variety of applications such as a wearable gesture recognizer [7, 23], a jamming/pinching/squeezing interface [11, 17, 47], and a smart textile for prosthetics [22] have been proposed. For flexible and effective sensing, previous works adopted soft materials to avoid the rigidity of the components. Still, it is hard to modify an already implemented design or instrument with multiple sensing modalities. In our work, we support flexibility in customizing the sensors as well as multimodal sensing using a single-volume material.

Electrical Impedance Tomography for Sensing Technique
Electrical impedance tomography (EIT) has been explored widely in the robotics field to implement artificial skin [41]. In particular, the EIT approach has enabled the tactile sensing without distributed sensory elements in the sensing area. This frees sensors from complex wirings and allows sensing with a single-volume material. By incorporating conductive materials, previous works have evolved the EIT sensing in terms

of robustness against stretching [3], the accuracy with neural learning [33], and affordance with various shapes [42]. Recent studies in HCI also employed EIT for gesture recognition with a wearable form factor [58] and enabling touch sensing on arbitrary surfaces [57]. However, previous approaches required additional material layers (e.g., conductive textile matrix) for real-time continuous tracking, which were susceptible to environmental noises, and did not support a fully stretchable interface. We utilize the EIT sensing technique to support real-time continuous contact and stretching in both flexible and stretchable form factors.

Carbon Elastomer for Sensing
Among the many available soft conductive materials, carbon-filled liquid silicone rubber has been used widely for sensing purpose. Since it possesses excellent piezoresistive properties to sense the mechanical deformations [29]. Previous researchers utilized carbon filled elastomer for recognizing and monitoring hand gestures [25], contact/force-sensing input pad [31, 38], breathing and speech [52], seat posture [10], and structural health [16]. However, the long settling time requirement after deformations and nonlinear characteristics hinder researchers from utilizing this material for real-time applications [25]. In particular, we focus on overcoming this issue for real-time contact localization. We propose a dynamic baseline update to use with the existing EIT techniques. The updates are controlled by fingertip contact and movement detections. Thus, we achieve real-time continuous contact sensing with a carbon filled elastomer.

Adding & Customizing Interactivity
The advances in electronics and sensors have promoted adding interactivity to objects. This process has been applied to 3D printed pieces and existing objects by retrofitting [34], visible annotations [39], capacitive sensing [40], magnetic sensing [56], and mobile devices [21]. To support an easily customizable interface, conductive inkjet printing [12, 19] and cuttable circuits [6, 28] have been suggested. To this end, these approaches involve easy and maturing fabrication processes such as 3D printing and 2D circuit printing. In terms of soft composite materials, previous researches have also demonstrated shape changing interfaces which incorporate external pneumatic actuation and auxiliary sensing components [11, 54]. However, because of the multi-step fabrication and multi-layer structure which are commonly used for soft sensors [50, 51], the customization has not been supported for the soft sensing based interfaces. Thus, we propose a workflow providing interface customization using soft sensors.

DESIGN GOALS AND CHALLENGES
Form Factor: With soft sensors, users can bring interactivity to stretchable, flexible, and deformable mediums such as desk lamps, clothing, and malleable and soft objects. Our proposed method should allow one to use soft materials to add natural interactions to objects. With carbon elastomer, both 2D thin sensor sheet and 3D soft sensor block can be implemented. For this paper, we emphasize the design and fabrication of thin soft sensors with customized 2D shapes which can be deployed alone or wrapped onto 3D objects.
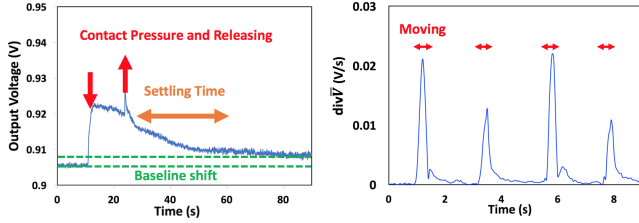
Figure 1. Voltage reading from a sensing channel fed with fixed DC current upon pressure (Left). Movement detection using $div\bar{\nabla}_i$ smoothed by a 5-frame running average (Right).

Sensing Capability: We aim to provide rich sensing capabilities while preserving the desired form factors. *iSoft* is designed to provide multimodal sensing including real-time contact and stretching. Allowing real-time contact sensing can bring touch pad capability (continuous tracking and 2D finger-tip gestures) using natural fingertip movements. To map natural motions and behaviors as a meaningful input, our approach also supports the multimodal sensing capability. For example, to sense actions such as stretching clothing and bending a flexible lamp arm with our hands, both contact sensing and stretching/bending sensing are required.

Fabrication and Implementation: A simple and a low-cost sensor fabrication is desirable to support users who have no professional material knowledge or expensive equipments. Our approach targets allowing HCI practitioners and hobbyists to quickly design and deploy their personalized interfaces with soft-matter sensors. Also, a customization toolkit for the hardware assembly guidance is needed to lower the barrier for implementing the soft sensors. Moreover, the toolkit should support a certain level of design freedom in a visual and intuitive manner. Further, the assembly process should be concise to reduce costs in the post-processing stage.

SENSING PRINCIPLE

Our contact sensing is based on the EIT technique which estimates the resistance distribution of the conductive material using inverse problem analysis based on measurements from the sensor boundary. The difficulty of providing real-time sensing with the carbon-filled silicone rubber is due to its rebound elasticity ($> 50\%$), which causes a long settling time ($> 10s$) and small shifts in baseline values as shown in Figure 1. In this section, we explain the resistance measurements method we used. Then, we show our approach to overcome previous difficulties and achieve real-time contact sensing with a carbon filled silicone rubber. Furthermore, we explain how other sensing modality (i.e., stretching) works.
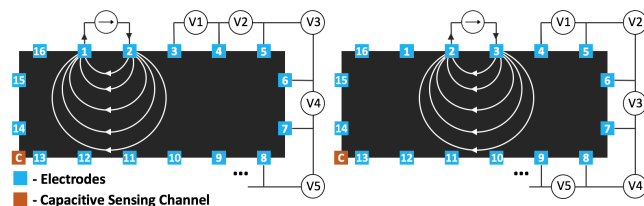

Figure 2. Four-terminal sensing employing the *Neighboring Method* with a capacitive sensing channel.
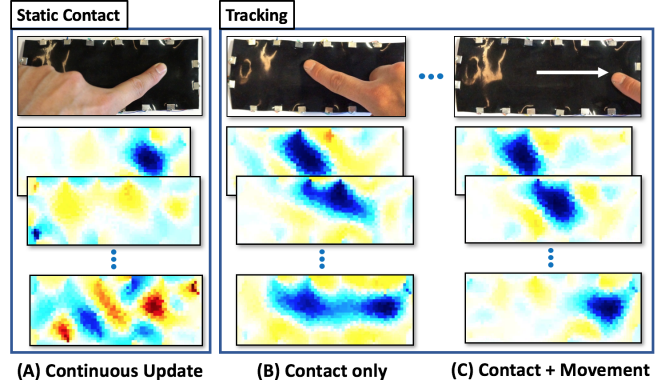

Figure 3. (A) Contact localizations through continuous update only lasts for a short amount of time. (B) Effects of residual deformations can be solved utilizing both fingertip contact and movement detections enabling (C) real-time contact sensing.

Resistance Measurement Method

Our sensing approach is based on carbon-filled silicone rubber which changes its resistance distribution upon mechanical deformations. Four-terminal sensing is used to measure resistance since this method reduces the inaccuracy from contact resistances. Unlike matrix tactile sensors where arrays of electrodes are required within the sensing area, we place sensing electrodes on the outer edge of the sensor. Then, we use *Neighboring Method* where DC current is fed through two adjacent electrodes and the voltage differential is measured successively throughout the adjacent electrode pairs as shown in Figure 2. Among the different pooling methods, the neighboring method has shown the highest selectivity [18] which is suited for implementing contact localization.

Real-time Contact Sensing with EIT

EIT image reconstruction is carried out by comparing the measurements at two different instances. Previous work showed discrete contact sensing using EIT with carbon elastomer by taking measurements under the initial no-load condition as a *constant baseline* [3]. However, a small shift in the reference baseline can easily distort the contact localization. Thus, the use of a constant baseline will not perform accurately if baseline shifts. Furthermore, the long settling time limits the applicability in dynamic situations such as fast discrete contacts and continuous movement. In order to eliminate the distortion and apply EIT for real-time contact sensing, we introduce a *dynamic baseline* update mechanism. Our baseline update mechanism emerges through following three steps:

1. Continuous Update: A simple approach would be using the *Fast EIT* [9] approach where the system updates the baseline values at every frame. However, this contact localization only lasts for a short amount of time ($<0.3s$) for piezoresistive materials as shown in Figure 3(A). The reason is that, if the baseline keeps refreshing every frame, the changes in voltage readings disappear once the fingertip stops creating new deformations (e.g., staying at the same location).

2. Contact Switch: From the observations on the *Fast EIT*, a fingertip contact switch is needed to update the baseline
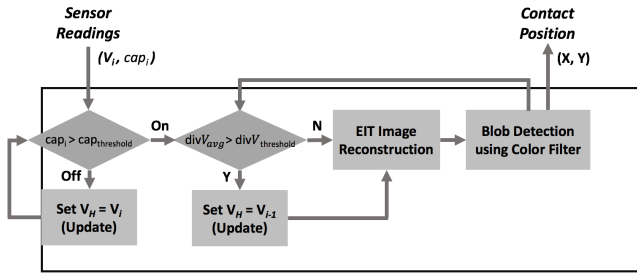
Figure 4. System flow of real-time continuous contact sensing.

properly. Once a contact is detected, the baseline stops updating and holds until the contact disappears. Thus, the contact localization remains valid even if the fingertip stays at the same location. So far, the performance of discrete contact localization becomes robust. However, during a continuous fingertip movement, the residual deformations on the path mark on the reconstructed images as a long stroke as shown in Figure 3(B). We detect fingertip contact robustly by adding an extra capacitive sensing channel (Figure 2) within the resistance measurement loop.

3. Contact + Movement Switches: Successively, if we can detect the finger movement and use it for a secondary level switch, real-time contact localization in continuous finger movement becomes feasible. While a fingertip remains in contact with the sensor, we initiate updating the baseline once a movement is detected and end updating when the movement stops. Therefore, the marks from the residual deformations are erased as in Figure 3(C). In our preliminary experiments, we observed that the average of all channels' instant measurements (V_{avg_i}) reflects a similar behavior with overall resistance distribution. To this extent, we use a discrete-time derivative $div\,V_{avg_i}$ as an indicator to detect a movement. Also, we apply a running average on $div\,V_{avg_i}$ for a stable and robust detection (Figure 1).

By utilizing the proposed two-step event detection for the dynamic baseline updating, we achieve real-time contact sensing system. Figure 4 illustrates the overall flowchart:

1. Update a homogeneous baseline data ($\mathbf{V}_H$) with instant measurement readings ($\mathbf{V}_i$, running average of recent 5 frames) while no contact is detected, i.e., the capacitive sensing value ($cap_i < cap_{threshold}$).

2. If $cap_i >= cap_{threshold}$, $\rightarrow$ movement detection process.

3. If a movement is not detected, i.e., $div V_{avg_i} < div V_{avg_{threshold}}$, $\rightarrow$ image reconstruction.
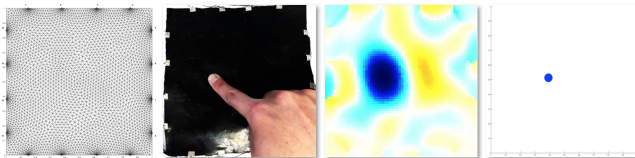
4. If $div V_{avg_i} >= div V_{avg_{threshold}}$, we update $\mathbf{V}_H$ with previous frame's data ($\mathbf{V}_{i-1}$) and $\rightarrow$ image reconstruction.

5. We apply a color filter to the reconstructed image for blob detection and localize a contact coordinate from the center of the blob (Figure 5).

With the proposed method, we can localize multiple contact points. However, the low-resolution of the reconstructed image allows multi-point contact sensing with a distinct separation greater than 5 cm.

Multimodal Sensing with Stretching
Our approach achieves a multimodal sensing with real-time contact and stretching. We employ a regression analysis to recognize different levels of stretching. We observed from our preliminary test that the stretching caused changes in all of the sensor values. Thus, as the first instantiation, we utilize V_{avg} for the regression analysis. The regression analysis result is further discussed in the **Task Evaluation** section. Since carbon elastomer shows hysteresis, which produces different resistance distributions under loading and unloading conditions [53], we only focus on stretching sensing under loading instances (pulling). An unloading condition can be detected since a high peak appears before decreasing to the settling value [25]. Since stretching along different axes exhibit different behaviors, they should be modeled separately. In this paper, we only showcase stretching along a single axis.

FABRICATION PROCESS
Material & Equipment: We employed a carbon-filled silicone liquid rubber from Wacker Ltd. [49] which exhibits similar volume resistivity (11 Ω·cm) as polymer sensors made with carbon nanotubes (1 $\sim$ 200 Ω·cm) [2]. The curing condition of the material is *15 minutes at 165°C* using compression molding. We proposed quick approaches either using a T-shirt heat press machine (<\$150) or a pair of tightly screwed steel blocks heated inside a toaster oven (<\$50) as shown in Figure 6(B). We used reusable heat stabilized film (\$1.7/sheet) to protect the surface from damage during curing. The current material cost of making a letter-sized sensor is about \$4.

Procedure: As shown in Figure 6(A), the process started with applying mixed two-part components of carbon-filled elastomer to the heat stabilized film using a palette knife. Based on the size and thickness requirement, users need to adjust

Figure 5. EIT technique based tracking workflow: Finite Element Model (Left), a 20×20 cm sensor, the reconstructed image, and tracking through blob detection (Right).
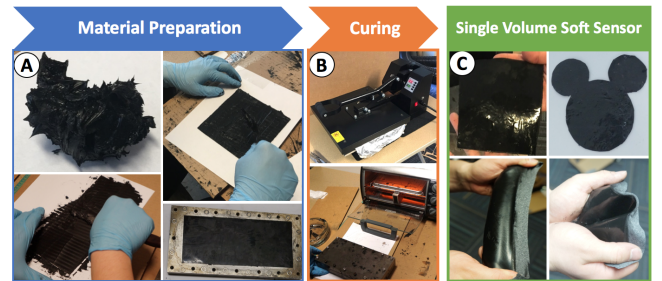

Figure 6. Simple material fabrication process: (A) Mixing and painting material and (B) curing them with either a T-shirt heat press or a toaster oven. This produces (C) various single-volume soft sensors.
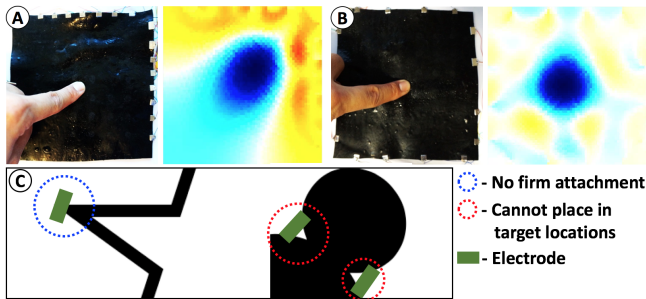
Figure 7. Potential electrode placement problems: Electrode placement (A) not enclosing a whole sensor region and (B) enclosing the whole area; (C) Improper electrodes placement on sharp edge corners.
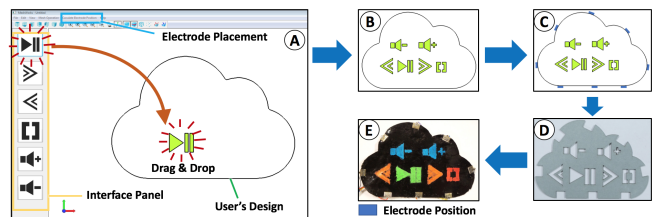

Figure 8. Proof-of-concept toolkit showing (A) overall interface, (B) interface customization, (C) electrode placement, (D) guidance template, and (E) prototype.

the volume of the elastomer. After putting another film on the other side, we used either a *T-shirt heat press* machine or *steel blocks+oven* to cure the material with constant pressure. We controlled the thickness of the material (>500 *μm*) by placing steel washers around the curing sample. In this paper, we used a thickness of 0.8 mm. The curing takes about 140 seconds and 60 minutes using a T-shirt heat press and a toaster oven, respectively. For the T-shirt heat press, we flipped the material at 70 s to apply uniform heat on both sides. It is worth noting that the material is sensitive to the curing durations where excessive durations cause *Scorching*. Therefore, the single volume sensor is fabricated with no additional material processing.

Supporting Form Factors: Our form factors include arbitrary 2D shapes and textiles (Figure 6(C)). To fabricate on textiles, we replace heat stabilized film with the textile materials.

CUSTOMIZATION AND DEPLOYMENT

Customization Toolkit

We develop a customization toolkit to support users in designing and deploying their own personalized interface with *iSoft* (Figure 8). The current EIT toolkit (*EIDORS*) requires users to manually input geometry information and electrode locations as a set of coordinates [48]. Using our toolkit, users can simply draw/import their own designs. Then the toolkit interfaces with the *EIDORS* by exporting boundary and electrode information. Lastly, it is critical to place electrodes in accordance with the simulation model since small discrepancies increase the error [46]. Thus, the toolkit generates a guidance image which users can refer to in designing the sensor and deploying electrodes.

Electrode Placement

There are two main factors we need to consider: 1) Placing electrodes with equal distances on the boundary of the given shape and 2) Avoiding sharp corners when placing the electrodes. First, not enclosing the whole sensor area shows unbalanced performance in localization among the different regions compared to the electrode placement with enclosing all the area (Figure 7(A, B)). We maintain equal distance between electrodes to guarantee enclosing all the sensor regions. Second, we avoided the sharp corners since they create singularity problems due to the Neumann boundary condition used in finite element analysis of the EIT [13]. In addition,

we prevent a situation where users could not place the electrodes properly (could not make full contacts or put electrodes in the designated locations) as shown in Figure 7(C). Thus, we design our customization toolkit to produce an electrode configuration that works with the EIT software toolkit which will be discussed in the **Implementation** section. To fulfill the two aforementioned requirements, we proposed an electrode placement algorithm as follows:

Initial electrode placement: All the points on a boundary curve are parameterized using arc length parameterization. Based on this parameterization, with a randomly chosen starting point, *N* evenly distributed electrode locations are generated in the parametric domain. The electrode number *N* is determined by the effective area of the interaction. In our test, we set *N* to be either 8 or 16. This initial electrode placement guarantees the even distribution of all electrodes.

Best electrode placement search: Based on the results of the initial electrode placement, we apply a search algorithm to find the best electrode placement which avoids placing the electrode onto the sharp corners on the boundary curve. The evaluation metric for the sharp corners is defined as follows:

$$Score = \sum_{i=1}^{N} \overline{chordal}(\Psi_{\mathbf{P}_i}), \qquad (1)$$

where $\mathbf{P}_i$ is each electrode location, $\Psi_{\mathbf{P}_i}$ is the set storing neighboring points of $\mathbf{P}_i$, and $\overline{chordal}(\cdots)$ measures the average chordal length error of all points in $\Psi_{\mathbf{P}_i}$. The number of $\mathbf{P}_i$'s neighbors to be added in $\Psi_{\mathbf{P}_i}$ is determined with a width $\omega \cdot l$, where l is the ribbon end size, and ω is a user specified factor. In all our experimental tests, ω is set to be 2.0. The search algorithm is designed to find a set of electrode locations with a minimum score evaluated by Eq.1. By rotating the boundary of curve at every small step δ in the parametric domain, we recursively parameterize the same boundary curve and evaluate the score to find the best electrode locations. Note that, the searching stops when the rotation reaches $\frac{2\pi}{N}$ degrees due to the rotational symmetry of the electrode locations. The rotation step angle δ is set to $\frac{0.04\pi}{N}$ for balancing the search resolution and the speed.

IMPLEMENTATION

Figure 9(A) illustrates our prototype including a sensor (20×7 cm, 0.8T) and sensing board. The dimensions of the sensing board were 5(W)×5(D)×3(H) cm.
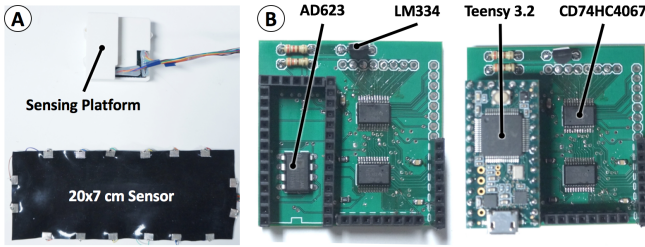
Figure 9. (A) EIT sensing board with the sensor and (B) customized 16-channel shield.

Electrode Connection

Once the sensor fabrication was done, electrodes should be installed on the periphery of the sensor to perform EIT sensing. Among the various available materials, we chose *Ribbon Crimp Ends* used in jewelry craft. These provided a firm contact with the sensor and easy installation/detachment. The wires were soldered onto the ribbon ends and provide connections between the sensor and the sensing board.

Hardware

Figure 9(B) shows our customized 16-channel shield operated with Teensy 3.2 (72 MHz Cortex-M4) [15]. The board contained an adjustable current source (LM334, Texas Instruments) for current injection and an instrumentation amplifier (AD623, Analog Devices). A total of four 16-to-1 multiplexers (CD74HC4067, Texas Instrument) were used to form a switching matrix. A pair of multiplexers connected current source and ground to the target electrodes. Another pair of multiplexers connected the voltage measurement electrodes to the instrumentation amplifier. The total cost of customized shield and microcontroller was $30. We consider the current dimensions and the cost as an upper limit which can be further reduced through commercial production.

Sampling & Data Acquisition

Figure 10 illustrates the schematic view of our prototype. The sampling was done in two steps: voltage measurements and capacitive sensing. The voltage measurements were amplified to maximize the dynamic range of the ADC reading. Teensy's ADC provides a 12-bit resolution and we modified ADC sampling setting to maximize the frame rate. When we injected the fixed current (<0.5 mA), we put 100 μs delay to provide sufficient time for the current to propagate before starting the
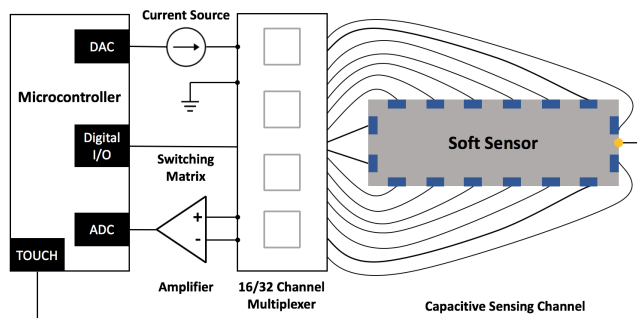

Figure 10. Schematic view of our system for 16 electrodes.

voltage measurements. We averaged 10 analog readings for a single voltage measurement (3 μs). At the end of the voltage reading cycle, we disabled all multiplexer channels and perform capacitive touch sensing through designated pin (Touch-Pin) in Teensy. We modified the current, a number of scans, and prescaler setting of the capacitive sensing to minimize the measurement time (<100 μs). The overall frame rate for the different number of electrodes (8,16, and 32) along with the capacitive sensing was investigated. To test the 32 channels, we used a customized 32-channel shield with four 32-to-1 multiplexers (ADG732, Analog Devices) and Teensy 3.2. We observed a low frame rate (13 Hz) using 32 channels due to the limited microcontroller clock speed. Since we are interested in real-time contact sensing, we focus on 8 and 16 electrodes.

Contact Localization

Our contact localization platform was developed based on the use of *EIDORS* EIT toolkit [48]. We performed contact localization on a 15" MacBook Pro with a 2.5 GHz Intel Core i7 processor. After preliminary explorations, our image reconstruction was formulated by a regularized *maximum a posteriori* [1] using *one step Gauss Newton solver*. More specifically, we fixed hyperparameter value at μ =0.01 which controlled the smoothing of the output along with *NOSER* prior. Similar to [58], we also had a pre-computation step during initialization (<3 s) where subsequent image reconstruction was carried out as a single matrix multiplication (2.5 *ms*). After forming a reconstructed image (25 *ms*), we set thresholds on the blue channel to compute the centroid of the effective region (0.5 *ms*). The frame rate of the EIT image reconstruction came out to 35 Hz when using 16 electrode configuration.

Stretching Sensing

For the stretching sensing, we employed a regression analysis to model the sensor behaviors upon stretching. We chose the average value from all channels ($\bar{\mathbf{V}}_i$) as a dependent variable since stretching the material changed the resistance distribution over the sensor area. Since the stretching sensing is a model based approach, the frame rate is similar to the sampling frame rate (> 50 Hz). We will discuss the details of the stretching model in the **Technical Evaluation** section.

TECHNICAL EVALUATION

To fully understand the performance of the proposed sensor, we devised our evaluation to explore all attributes that affect the sensor performance. In particular, we evaluated the contact localization performance with different sensor sizes, a number of electrodes, and stretching conditions. Moreover, we modeled one case of stretching sensing using a regression analysis to confirm the feasibility.

Experiment I: Contact Localization

In this evaluation, we investigated 1) the required force to activate the sensor, 2) the sensor sizes, and 3) the number of electrodes for their effects on the contact localization performance. We employed a discrete targeting method where we compared the distance error of each contact with the ground truth. We used a digital force gauge with a flat conductive head ($\varnothing$15 *mm*, similar to a fingertip size) as a targeting
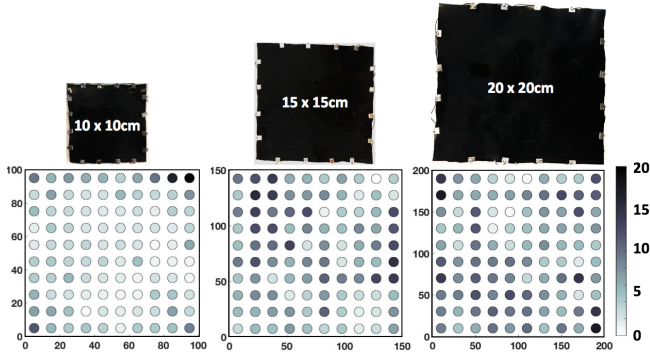
Figure 11. Targeting accuracy on three different sensor sizes with 16-electrode configuration as shown in mm.

Figure 12. Targeting accuracy on three different sensor sizes with 8-electrode configuration as shown in mm.

medium. To guide accurate contact locations, we attached a printed 10×10 grid paper with cut holes which dissected each sensor into 100 contact regions. Each region was pressed manually 5 times in a random order. In each trial, we averaged 50 readings for a single measurement. We collected 6000 data points (100 locations×3 sensor sizes×2 electrode configurations).

Contact Force Requirement: Prior to the targeting experiment, we preliminarily evaluated the contact force requirement for targeting the contact localization. We tested with three sensor sizes (10×10 cm, 15×15 cm, and 20×20 cm) with a 16-electrode configuration. We measured the force required to activate the contact sensing at each grid location. The system logged the force from the digital force gauge when a contact sensing was activated. We observed that the required force increased as the contact distance increased from the electrodes. The threshold contact forces were in a range of 0.97∼2.8 N which is considered to be a comfortable fingertip force range for pressing [26]. This result shows that users do not need to put excessive efforts into activating the contact sensing. It is worth noting that *iSoft* was still capable of localizing contact with a contact force exceeding the threshold range.

Sensor Size: We tested the contact localization accuracy on 3 different sized sensors (10×10 cm, 15×15 cm, and 20×20 cm) with a 16-electrode configuration. We scaled the 10×10 grid to different sensor sizes accordingly, which resulted in a grid size of 10×10 mm,15×15 mm, and 20×20 mm. The average targeting errors were 3.8 mm (SD=2.89), 6.89 mm (SD=3.63), and 7.53 mm (SD=3.49) for 10×10 cm, 15×15 cm, and 20×20 cm respectively. As shown in Figure 11, we found that some locations near the electrodes showed higher errors. We saw improvements of 10∼30% in distance errors when focusing on 80% of the center area for each sensor size.

Number of Electrodes: We performed another experiment with an 8-electrode configuration for the same sensor sizes. As mentioned before, 32-electrode configuration was not considered due to the low frame rate. As shown in Figure 12, the average targeting errors were 9.89 mm (SD=7.09), 16.34 mm (SD=8.54), and 18.41 mm (SD=13.51) for 10×10 cm, 15×15 cm, and 20×20 cm sensor sizes. Compared with the results from the 16-electrode setup, the overall errors increased. In particular, we observed that the outer re-
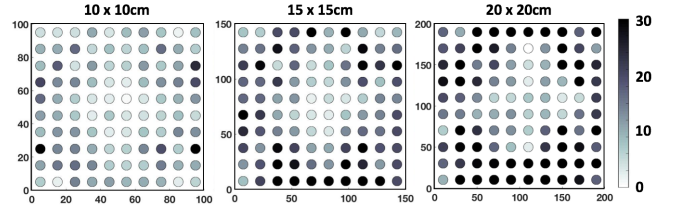
gion showed much worse performance in localization. If we had only considered the accuracy in the center area (80%), similar accuracies (<10% difference) as the 16 electrode configuration would have been achieved. This implied that a small number of electrodes can be employed for larger sensors if the center area is utilized as an effective sensing region. To fully utilize the whole sensor area, a greater number of electrodes is recommended.

Experiment 2: Sensor Performance with Stretching
We evaluated the characteristics of our sensor with stretching to check the feasibility of employing a stretching under loading conditions as an input. Prior to testing each parameter, we checked the maximum strain range for the stretching. This ensured that we performed evaluations in a feasible sensing range. We observed that the resistivity increased up to a 50% strain, but started to decrease above this region. With this finding, we confined our maximum strain range to 0∼40% for all evaluations. In this experiment, we used a sample size of 20×8 cm with 16-electrode configuration.

Previous work demonstrated that the carbon filled elastomer changes its resistivity non-reversibly after the first few stretches [53] due to a breakdown of the internal carbon black network. In our evaluation, we stretched the sensor up to 40% and back to 0%. We measured the resistance at the two ends along the stretching direction of the sensor after conducting 1, 5, 10, 50, 100, 500, and 1000 stretches operating at a frequency of 0.5 Hz. Before the next set of stretching, we left the sensor unloaded for sufficient amount of time (>1 day) to minimize the effect of the recovery rate in this experiment. As shown in Figure 13(A), a sharp increase in resistance was observed after the first few stretches. After 50 stretches, no substantial change in sensor reading was observed. This result indicates that the sensor should be stretched at least 50 times before deployment to ensure a uniform performance during
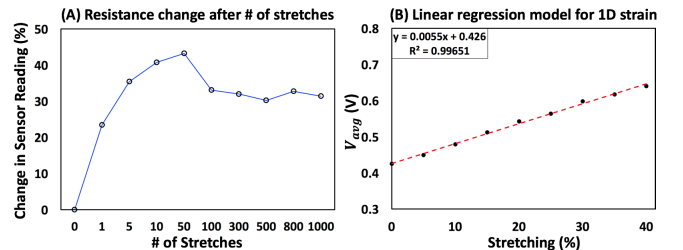

Figure 13. (A) Sensor durability undergoing a number of stretches and (B) a regression model for unidirectional stretching.
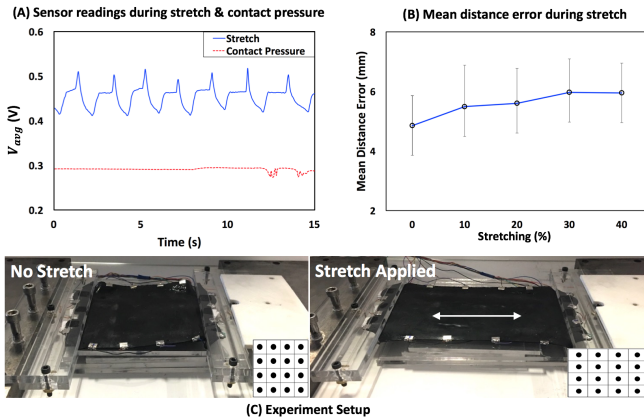
Figure 14. (A) Sensor reading during dynamic stretches and contact sensing, (B) contact localization performance under stretching, and (C) experiment setup showing 0% and 40% stretches.

stretching. Thus, we performed all further experiments with samples that underwent at least 50 cycles stretches.

For regression analysis, we used the average of measurements from all channels (V_{avg}) for the modeling. As previously mentioned, the hysteresis behavior of the sensor makes it hard to perform bi-directional stretching sensing. Therefore, we modeled the stretching at loading instance only for unidirectional stretching. Figure 13(B) illustrates a linear regression model with our sensor. Here, we stretched the sensor for a range between 0~40% for every 5%. We stretched the sensor from the released condition for the data collection. This shows the feasibility of using our prototype for stretching sensing with different magnitude ($R^2 = 0.97$). We further evaluated stretching with users in the **Task Evaluation** section to see how many different magnitude levels can be used for inputs. It is worth noting that the different directional stretching should be modeled separately.

Experiment 3: Multimodal Sensing
In this experiment, we focused on multimodal sensing performance with contact sensing and stretching since the proposed prototype will mainly utilize these modalities for applications. First, we investigated sensor behavior during dynamic stretching and compared to sensing values from contact sensing. Then, we looked at contact sensing performance under different stretching conditions. We used a sensor size of 10×10 cm with 16 electrode configuration.

To test the contact localization under stretching, we designed a test jig (Figure 14(C)) where we applied a unidirectional strain between 0~40%. Here, we used a printed 4×4 grid paper scaled along the stretched direction where each grid is 2 cm square with the cut hole at the center. We used different sized grids according to the different stretching levels. Figure 14(B) illustrates the mean distance errors on 16 locations at different strain values. The result shows a slight increase in errors for higher strains from 4.85 mm to 5.95 mm. This confirms that contact localizations can still be employed in various stretching conditions.
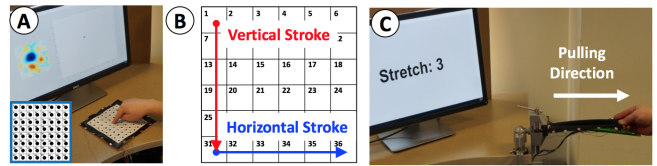

Figure 15. The overall study setup for (A) discrete contact, (B) stroke tracing (i.e.,q 15×15 cm sensor) and (C) stretching control tasks.

We compared V_{avg} under different excitations: contact press and finger movement versus stretching. Figure 14(A) demonstrates the sensor performance under dynamic stretches. The result shows that the sensor readings during the contact sensing were less than the sensor readings for a 10% stretch. To prevent the sensor from an unintentional trigger due to the contact pressure, we suggest utilizing the stretching range above 10% for inputs.

TASK EVALUATION
To further verify the system performance with real users, we conducted three task evaluations including discrete contact, stroke tracing, and stretching controllability. For all our evaluations, we used a 16-electrode configuration. We recruited 10 participants with a mean age of 26. Prior to each trial set, we offered a practice session to reduce the learning effect. However, it is worth noting that possible learning effects may still apply across different tasks.

Task1: Discrete Contact
We studied the system accuracy of the discrete targeting and the absolute positioning. We looked at whether the contact localization was robust across different users.

Setup: We evaluated users with three different sensor sizes as in our previous experiments. We chose a grid size of 2×2 cm to mimic the size of the common keycaps. Based on the technical evaluations, we utilized the center region as the effective sensing region which was 80% of the whole sensor area. More specifically, we applied 16, 36, and 64 contact locations on different sensor sizes accordingly. We randomized the order of both sensor sizes and contact locations. A total of 1500 data points were collected (50 trials×3 sensor sizes×10 users). We measured the accuracy of the grid targeting and the absolute positioning.

Result: As shown in Figure 16(A), the average of the discrete targeting accuracy was 96.03% and the distance error was
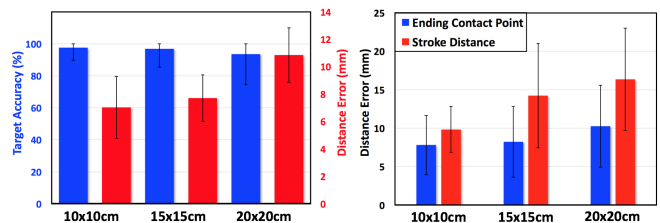

Figure 16. An accuracy of targeting 2×2 cm grid space and absolute position error during discrete contacts (Left), and distance errors for stroke distance and ending contact point (Right) on the three sensor sizes.
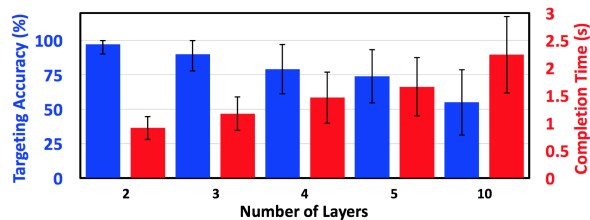
Figure 17. The targeting accuracy and completion time for controlling stretching with 5 different resolutions.

8.53 mm (SD=1.98) for all three sizes. Using repeated measures ANOVA for univariate analysis, there was no significant difference among the targeting accuracies, but there existed significant difference among distance errors ($F_{(2,18)}$=20.97, p<0.05). The post-hoc pairwise comparisons with Bonferroni correction showed significantly different distance errors between the 20×20 cm sensor size and the other sizes (p<0.05). We evaluated all sensor regions without employed machine learning models. Comparing with closest related work [57], our results showed similar performance for discrete contact sensing. The high targeting accuracies across all sensor sizes indicate that *iSoft* supports robust discrete contact localizations for instant interactions.

Task2: Stroke Tracing
We explored the system accuracy on the continuous contact sensing. We looked at the continuous contact localization using fingertip movement detection with users.

Setup: With the same sensors in **Task1**, we designed a stroke tracing task to evaluate the performance of our fingertip movement detection. We asked users to trace pre-defined strokes with fixed length on the soft sensors. For different sensor sizes, users traced different lengths (60, 100, 140 mm) both horizontally and vertically for each column and row (Figure 15(B)). We randomized the order of both sensor sizes and tracing distances. A total of 1080 data points were collected (18 stroke instances×2 directions×3 sensor sizes×10 users). We measured the absolute position at the ending contact point of the tracing and the stroke distances.

Result: Figure 16(B) shows that the average distance errors were 8.76 mm (SD=4.59) for the ending contact points and 13.48 mm (SD=5.74) for the stroke distance in all sensor sizes. Compared to **Task1**'s result, we did not observe a significant difference in the distance errors in the ending location of the tracing. This confirms that the fingertip movement detection worked robustly across different users' strokes. As expected, the stroke distance error was bigger than the ending point contact localization since we used both starting and ending points to compute the distance. It is worth noting that the stroke distance errors were less than 10% of the sensor sizes. This shows that *iSoft* supports continuous contact sensing.

Task3: Stretching Controllability
We evaluated the participant's targeting controllability with stretching using our prototype. Our goal was to confirm how many stretching resolutions users can handle with our sensor. We measured both accuracy and reaction time.
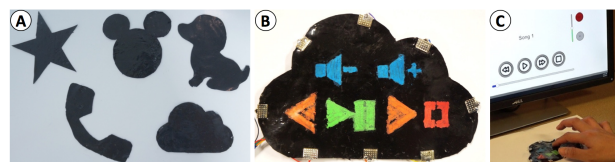

Figure 18. *iSoft* enables a personalized interface with 2D shapes.

Setup: We evaluated users' target controllability with a stretching range of 20~40% on five different resolutions (i.e. evenly dissecting a total sensing range into 2,3,4,5, and 10 layers). The target was labeled as a number from 0 (No Stretching) to the maximum range (2~10 levels) which was displayed on the screen as a reference. We asked users to stretch the material to the designated target within one unidirectional stretching. This way, users could not adjust the input by stretching and releasing. Participants then released the sensor fully before the next trial. We randomized the order of resolutions and collected a total of 1000 data points (20 trials×5 layers×10 participants).

Result: As shown in Figure 17, the participants achieved an average accuracy of more than 90% in controlling 3 or fewer levels of stretching in both conditions. However, the performance quickly dropped starting from 4 or more levels (<75%). Also, the completion time increase as the resolution grew. This shows that even with the high stretching capability of *iSoft*, it is recommended to limit the interaction resolutions of 3 or fewer levels for robust interactions.

EXAMPLE APPLICATIONS
We highlight the multimodal sensing capability and the interactions enabled by the real-time contact and stretching sensing with *iSoft*. The following examples demonstrate the wide range of flexibility and applicability of *iSoft*.

Customizable 2D Soft Sensor Accessory: A user can cut various shapes from a fabricated sheet and color them with paint markers to create customized soft sensors (Figure 18). These sensors can be used as controllers for various digital devices. The sensors work instantly with discrete/continuous contact sensing capability.

Lamp Arm: We wrapped a 15×6 cm sensor on to the adjustable arm (Figure 19) with 8 electrode configuration. The arm of the lamp became capable of sensing bending, discrete contact, and swiping. In this example, users simply turned on the lamp by bending the arm and controlled the brightness using different arm locations. This example demonstrates the versatile sensing capability of *iSoft*.
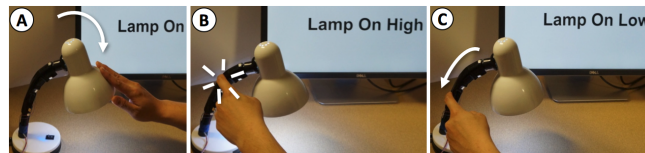

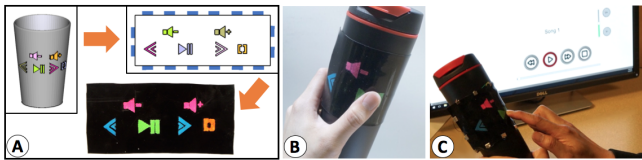**Figure 19. By attaching *iSoft*, we bring interactivity to a lamp arm.**

Figure 20. Users design a personalized interface sticker for a tumbler.

Add-on Interactive Sticker for a Tumbler: Using our sensor and the toolkit, users can build their own soft interface for a Tumbler (Figure 20). Users can customize interfaces and the toolkit automatically generates the interface layout onto a 2D rectangular pattern and creates a guide for users to build a soft sensor sticker. The fabricated sensor can be attached onto the cup with adhesives and the tumbler instantly turns into a personalized music controller.
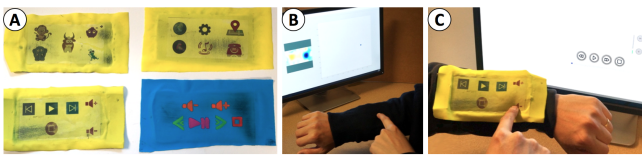

Figure 21. *iSoft* brings multimodal sensing capability for the textile.

Smart Textile Controller: We fabricated textile sensors and decorated them with fabric transfer paper and paint markers (Figure 21). The sensor can be attached either outside or inside, and a user can use the smart textile as a wearable controller. Various parts of clothing can become interactive such as sleeves and pockets.
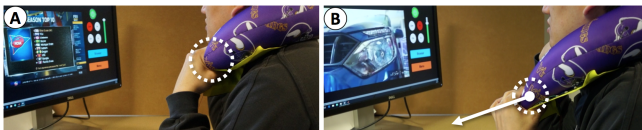

Figure 22. An interactive pillow provides a TV interface control.

Neck Pillow TV Control: The sensor can be attached or embedded in a volumetric fabric such as neck pillow. In this example, a user can control the channel by pressing different parts of the pillow and the volume by pressing+stretching different sides of the pillow. This demonstrates the use of the multimodal sensing capability utilizing a user's natural motions. A user can also further stretch the pillow for faster volume change.

DISCUSSION & FUTURE WORK

Although the fabrication processes, sensing techniques, and work flow we presented with *iSoft* suffice our design goals in general, we identify several challenges learned from the investigation. We discuss these challenges and future works.

Scalability & Form Factor: In our current setting, our physical sensor size is limited. However, the sensor can be fabricated using an industrial heat compression machine for larger working areas. For such constraints, more electrodes are recommended for robust performance. Further, applying our soft

sensors conformally onto complex 3D surfaces remains unresolved. The potential solution would be providing a feature of flattening complex 3D surfaces into 2D pieces [20].

Customization Freedom: Since *iSoft* is constructed with a carbon-based material, the base color is pure black. In our current approach, we colored it with paint markers which can be damaged with excessive stretching. A future approach would be using special silicone inks [45].

Supporting Other Sensing Modalities. We also saw the potential of using *iSoft* for other sensing modalities such as bending, squeezing, and contact pressure. We observed promising results to recognize bending along different directions using an ad-hoc training approach on a 10×10 cm sensor.

EIT Performance:The electrode connections can be further improved by incorporating long protrusions on the sensors for placing the electrode [31]. We can further improve the localization accuracy by with improved meshing model, enhanced blob detection, and optimized electrode placement.

Capacitive Sensing: Our current approach is limited to interactions through the conductive medium like human skin since we employed capacitive sensing. The localization still works with conductive materials if the electrodes are isolated.

The employed capacitive sensing does not indicate the material's viscoelastic response. However, as long as sufficient deformation happens during the on/off state transition period, localization works robustly. We confirmed that there is no performance degradation unless users repeatedly contact the same location with high frequency (> 5Hz), which usually is not the case for common interactions.

Stretching Performance: In this paper, we showed stretching under loading conditions only due to the hysteresis. By modeling the hysteresis, it is possible to achieve stretching sensing under both loading and unloading conditions.Our prototype supports up to 1 Hz stretching due to the settling time, which can fulfill most of the commonly used interactions.

Calibration Process: For capacitive, movement, and stretching sensing, initial calibrated data/models are required. By collecting sensor designs (size and material properties) and calibrated thresholds/models across the community, we expect generalized and shareable models can be developed.

CONCLUSION

We have proposed a customizable soft sensor, *iSoft*, with multimodal sensing for instant interactions. By employing a dynamic baseline update to the EIT technique using fingertip contact and movement detection, we have achieved real-time continuous contact sensing. *iSoft* also provides multimodal sensing capability with stretching sensing. We have developed a software toolkit that facilitates the customization and deployment process for implementing a functional soft sensor with the personalized interface. We also have verified the system accuracy and evaluated user performance. Our work will benefit HCI practitioners and novice makers who want to make their own functional soft sensors without in-depth knowledge on material processing or expensive fabrication equipment.

REFERENCES
1. Andy Adler and Robert Guardo. 1996. Electrical impedance tomography: regularized imaging and contrast detection. *IEEE Transactions on Medical Imaging* 15, 2 (Apr 1996), 170–179. `http://doi.org/10.1109/42.491418`

2. Alamusi, Ning Hu, Hisao Fukunaga, Satoshi Atobe, Yaolu Liu, and Jinhua Li. 2011. Piezoresistive Strain Sensors Made from Carbon Nanotubes Based Polymer Nanocomposites. *Sensors* 11, 11 (2011), 10691–10723. `http://www.mdpi.com/1424-8220/11/11/10691`

3. Hassan Alirezaei, Akihiko Nagakubo, and Yasuo Kuniyoshi. 2007. A highly stretchable tactile distribution sensor for smooth surfaced humanoids. In *2007 7th IEEE-RAS International Conference on Humanoid Robots*. 167–173. `http://doi.org/10.1109/ICHR.2007.4813864`

4. Chin-yu Chien, Rong-Hao Liang, Long-Fei Lin, Liwei Chan, and Bing-Yu Chen. 2015. FlexiBend: Enabling Interactivity of Multi-Part, Deformable Fabrications Using Single Shape-Sensing Strip. In *Proceedings of the 28th Annual ACM Symposium on User Interface Software and Technology (UIST '15)*. ACM, New York, NY, USA, 659–663. `http://doi.org/10.1145/2807442.2807456`

5. Alex Chortos, Jia Liu, and Zhenan Bao. 2016. Pursuing prosthetic electronic skin. *Nature Materials* 15, 9 (2016), 937–950. `http://doi.org/10.1038/nmat4671`

6. Artem Dementyev, Hsin-Liu (Cindy) Kao, and Joseph A. Paradiso. 2015. SensorTape: Modular and Programmable 3D-Aware Dense Sensor Network on a Tape. In *Proceedings of the 28th Annual ACM Symposium on User Interface Software and Technology (UIST '15)*. ACM, New York, NY, USA, 649–658. `http://doi.org/10.1145/2807442.2807507`

7. Artem Dementyev and Joseph A. Paradiso. 2014. WristFlex: Low-power Gesture Input with Wrist-worn Pressure Sensors. In *Proceedings of the 27th Annual ACM Symposium on User Interface Software and Technology (UIST '14)*. ACM, New York, NY, USA, 161–166. `http://doi.org/10.1145/2642918.2647396`

8. Paul H. Dietz, Benjamin Eidelson, Jonathan Westhues, and Steven Bathiche. 2009. A Practical Pressure Sensitive Computer Keyboard. In *Proceedings of the 22nd Annual ACM Symposium on User Interface Software and Technology (UIST '09)*. ACM, New York, NY, USA, 55–58. `http://doi.org/10.1145/1622176.1622187`

9. Peter M. Edic, Gary J. Saulnier, Jonathan C. Newell, and David Isaacson. 1995. A real-time electrical impedance tomograph. *IEEE Transactions on Biomedical Engineering* 42, 9 (Sept 1995), 849–859. `http://doi.org/10.1109/10.412652`

10. Marcello Ferro, Giovanni Pioggia, Alessandro Tognetti, Nicola Carbonaro, and Danilo De Rossi. 2009. A Sensing Seat for Human Authentication. *IEEE Transactions on Information Forensics and Security* 4, 3 (Sept 2009), 451–459. `http://doi.org/10.1109/TIFS.2009.2019156`

11. Sean Follmer, Daniel Leithinger, Alex Olwal, Nadia Cheng, and Hiroshi Ishii. 2012. Jamming User Interfaces: Programmable Particle Stiffness and Sensing for Malleable and Shape-changing Devices. In *Proceedings of the 25th Annual ACM Symposium on User Interface Software and Technology (UIST '12)*. ACM, New York, NY, USA, 519–528. `http://doi.org/10.1145/2380116.2380181`

12. Nan-Wei Gong, Jürgen Steimle, Simon Olberding, Steve Hodges, Nicholas Edward Gillian, Yoshihiro Kawahara, and Joseph A. Paradiso. 2014. PrintSense: A Versatile Sensing Technique to Support Multimodal Flexible Surface Interaction. In *Proceedings of the SIGCHI Conference on Human Factors in Computing Systems (CHI '14)*. ACM, New York, NY, USA, 1407–1410. `http://doi.org/10.1145/2556288.2557173`

13. LJ Gray and E Lutz. 1990. On the treatment of corners in the boundary element method. *J. Comput. Appl. Math.* 32, 3 (1990), 369–386. `http://doi.org/10.1016/0377-0427(90)90043-Y`

14. Jaehyun Han, Jiseong Gu, and Geehyuk Lee. 2014. Trampoline: A Double-sided Elastic Touch Device for Creating Reliefs. In *Proceedings of the 27th Annual ACM Symposium on User Interface Software and Technology (UIST '14)*. ACM, New York, NY, USA, 383–388. `http://doi.org/10.1145/2642918.2647381`

15. PJRC Inc. 2017. Product Detail. (2017). Retrieved April 1, 2017 from `http://www.pjrc.com/teensy/index.html`.

16. Inpil Kang, Mark J Schulz, Jay H Kim, Vesselin Shanov, and Donglu Shi. 2006. A carbon nanotube strain sensor for structural health monitoring. *Smart Materials and Structures* 15, 3 (2006), 737. `http://doi.org/10.1088/0964-1726/15/3/009`

17. Thorsten Karrer, Moritz Wittenhagen, Leonhard Lichtschlag, Florian Heller, and Jan Borchers. 2011. Pinstripe: Eyes-free Continuous Input on Interactive Clothing. In *Proceedings of the SIGCHI Conference on Human Factors in Computing Systems (CHI '11)*. ACM, New York, NY, USA, 1313–1322. `http://doi.org/10.1145/1978942.1979137`

18. Pasi Kauppinen, Jari Hyttinen, and Jaakko Malmivuo. 2006. Sensitivity distribution visualizations of impedance tomography measurement strategies. *International Journal of Bioelectromagnetism* 8, 1 (2006), 1–9.

19. Yoshihiro Kawahara, Steve Hodges, Benjamin S. Cook, Cheng Zhang, and Gregory D. Abowd. 2013. Instant Inkjet Circuits: Lab-based Inkjet Printing to Support Rapid Prototyping of UbiComp Devices. In *Proceedings of the 2013 ACM International Joint Conference on Pervasive and Ubiquitous Computing (UbiComp '13)*. ACM, New York, NY, USA, 363–372. `http://doi.org/10.1145/2493432.2493486`

20. Tsz-Ho Kwok, Charlie CL Wang, Dongping Deng, Yunbo Zhang, and Yong Chen. 2015. Four-dimensional printing for freeform surfaces: Design optimization of origami and kirigami structures. *Journal of Mechanical Design* 137, 11 (2015), 111413. `http://doi.org/10.1115/1.4031023`

21. David Ledo, Fraser Anderson, Ryan Schmidt, Lora Oehlberg, Saul Greenberg, and Tovi Grossman. 2017. Pineal: Bringing Passive Objects to Life with Embedded Mobile Devices. In *Proceedings of the 2017 CHI Conference on Human Factors in Computing Systems (CHI '17)*. ACM, New York, NY, USA, 2583–2593. `http://doi.org/10.1145/3025453.3025652`

22. Joanne Leong, Patrick Parzer, Florian Perteneder, Teo Babic, Christian Rendl, Anita Vogl, Hubert Egger, Alex Olwal, and Michael Haller. 2016. proCover: Sensory Augmentation of Prosthetic Limbs Using Smart Textile Covers. In *Proceedings of the 29th Annual Symposium on User Interface Software and Technology (UIST '16)*. ACM, New York, NY, USA, 335–346. `http://doi.org/10.1145/2984511.2984572`

23. Jhe-Wei Lin, Chiuan Wang, Yi Yao Huang, Kuan-Ting Chou, Hsuan-Yu Chen, Wei-Luan Tseng, and Mike Y. Chen. 2015. BackHand: Sensing Hand Gestures via Back of the Hand. In *Proceedings of the 28th Annual ACM Symposium on User Interface Software and Technology (UIST '15)*. ACM, New York, NY, USA, 557–564. `http://doi.org/10.1145/2807442.2807462`

24. Darren J. Lipomi, Michael Vosgueritchian, Benjamin C-K. Tee, Sondra L. Hellstrom, Jennifer A. Lee, Courtney H. Fox, and Zhenan Bao. 2011. Skin-like pressure and strain sensors based on transparent elastic films of carbon nanotubes. *Nature nanotechnology* 6, 12 (2011), 788–792. `http://doi.org/10.1038/nnano.2011.184`

25. F. Lorussi, Enzo Pasquale Scilingo, M. Tesconi, A. Tognetti, and D. De Rossi. 2005. Strain sensing fabric for hand posture and gesture monitoring. *IEEE Transactions on Information Technology in Biomedicine* 9, 3 (Sept 2005), 372–381. `http://doi.org/10.1109/TITB.2005.854510`

26. Sachi Mizobuchi, Shinya Terasaki, Turo Keski-Jaskari, Jari Nousiainen, Matti Ryynanen, and Miika Silfverberg. 2005. Making an Impression: Force-controlled Pen Input for Handheld Devices. In *CHI '05 Extended Abstracts on Human Factors in Computing Systems (CHI EA '05)*. ACM, New York, NY, USA, 1661–1664. `http://doi.org/10.1145/1056808.1056991`

27. Vinh P. Nguyen, Sang Ho Yoon, Ansh Verma, and Karthik Ramani. 2014. BendID: Flexible Interface for Localized Deformation Recognition. In *Proceedings of the 2014 ACM International Joint Conference on Pervasive and Ubiquitous Computing (UbiComp '14)*. ACM, New York, NY, USA, 553–557. `http://doi.org/10.1145/2632048.2636092`

28. Simon Olberding, Nan-Wei Gong, John Tiab, Joseph A. Paradiso, and Jürgen Steimle. 2013. A Cuttable Multi-touch Sensor. In *Proceedings of the 26th Annual ACM Symposium on User Interface Software and Technology (UIST '13)*. ACM, New York, NY, USA, 245–254. `http://doi.org/10.1145/2501988.2502048`

29. Steve Park, Michael Vosguerichian, and Zhenan Bao. 2013. A review of fabrication and applications of carbon nanotube film-based flexible electronics. *Nanoscale* 5, 5 (2013), 1727–1752. `http://doi.org/10.1039/C3NR33560G`

30. Yong-Lae Park, Bor-Rong Chen, and Robert J. Wood. 2012. Design and Fabrication of Soft Artificial Skin Using Embedded Microchannels and Liquid Conductors. *IEEE Sensors Journal* 12, 8 (2012), 2711–2718. `http://doi.org/10.1109/JSEN.2012.2200790`

31. Pedro Piacenza, Yuchen Xiao, Steve Park, Ioannis Kymissis, and Matei Ciocarlie. 2016. Contact localization through spatially overlapping piezoresistive signals. In *2016 IEEE/RSJ International Conference on Intelligent Robots and Systems (IROS)*. 195–201. `http://doi.org/10.1109/IROS.2016.7759055`

32. Ivan Poupyrev, Nan-Wei Gong, Shiho Fukuhara, Mustafa Emre Karagozler, Carsten Schwesig, and Karen E. Robinson. 2016. Project Jacquard: Interactive Digital Textiles at Scale. In *Proceedings of the 2016 CHI Conference on Human Factors in Computing Systems (CHI '16)*. ACM, New York, NY, USA, 4216–4227. `http://doi.org/10.1145/2858036.2858176`

33. Ganna Pugach, Alexandre Pitti, and Philippe Gaussier. 2015. Neural learning of the topographic tactile sensory information of an artificial skin through a self-organizing map. *Advanced Robotics* 29, 21 (2015), 1393–1409. `http://doi.org/10.1080/01691864.2015.1092395`

34. Raf Ramakers, Fraser Anderson, Tovi Grossman, and George Fitzmaurice. 2016. RetroFab: A Design Tool for Retrofitting Physical Interfaces Using Actuators, Sensors and 3D Printing. In *Proceedings of the 2016 CHI Conference on Human Factors in Computing Systems (CHI '16)*. ACM, New York, NY, USA, 409–419. `http://doi.org/10.1145/2858036.2858485`

35. Gonzalo Ramos, Matthew Boulos, and Ravin Balakrishnan. 2004. Pressure Widgets. In *Proceedings of the SIGCHI Conference on Human Factors in Computing Systems (CHI '04)*. ACM, New York, NY, USA, 487–494. `http://doi.org/10.1145/985692.985754`

36. Christian Rendl, David Kim, Patrick Parzer, Sean Fanello, Martin Zirkl, Gregor Scheipl, Michael Haller, and Shahram Izadi. 2016. FlexCase: Enhancing Mobile Interaction with a Flexible Sensing and Display Cover. In

Proceedings of the 2016 CHI Conference on Human Factors in Computing Systems (CHI '16). ACM, New York, NY, USA, 5138–5150. `http://doi.org/10.1145/2858036.2858314`

37. Peter Roberts, Dana D. Damian, Wanliang Shan, Tong Lu, and Carmel Majidi. 2013. Soft-matter capacitive sensor for measuring shear and pressure deformation. In *2013 IEEE International Conference on Robotics and Automation*. 3529–3534. `http://doi.org/10.1109/ICRA.2013.6631071`

38. Ilya Rosenberg and Ken Perlin. 2009. The UnMousePad: An Interpolating Multi-touch Force-sensing Input Pad. In *ACM SIGGRAPH 2009 Papers (SIGGRAPH '09)*. ACM, New York, NY, USA, Article 65, 9 pages. `http://doi.org/10.1145/1576246.1531371`

39. Valkyrie Savage, Sean Follmer, Jingyi Li, and Björn Hartmann. 2015. Makers' Marks: Physical Markup for Designing and Fabricating Functional Objects. In *Proceedings of the 28th Annual ACM Symposium on User Interface Software and Technology (UIST '15)*. ACM, New York, NY, USA, 103–108. `http://doi.org/10.1145/2807442.2807508`

40. Martin Schmitz, Mohammadreza Khalilbeigi, Matthias Balwierz, Roman Lissermann, Max Mühlhäuser, and Jürgen Steimle. 2015. Capricate: A Fabrication Pipeline to Design and 3D Print Capacitive Touch Sensors for Interactive Objects. In *Proceedings of the 28th Annual ACM Symposium on User Interface Software and Technology (UIST '15)*. ACM, New York, NY, USA, 253–258. `http://doi.org/10.1145/2807442.2807503`

41. David Silvera-Tawil, David Rye, Manuchehr Soleimani, and Mari Velonaki. 2015. Electrical Impedance Tomography for Artificial Sensitive Robotic Skin: A Review. *IEEE Sensors Journal* 15, 4 (April 2015), 2001–2016. `http://doi.org/10.1109/JSEN.2014.2375346`

42. David Silvera-Tawil, David Rye, and Mari Velonaki. 2012. Interpretation of the modality of touch on an artificial arm covered with an EIT-based sensitive skin. *The International Journal of Robotics Research* 31, 13 (2012), 1627–1641. `http://doi.org/10.1177/0278364912455441`

43. Ronit Slyper, Ivan Poupyrev, and Jessica Hodgins. 2011. Sensing Through Structure: Designing Soft Silicone Sensors. In *Proceedings of the Fifth International Conference on Tangible, Embedded, and Embodied Interaction (TEI '11)*. ACM, New York, NY, USA, 213–220. `http://doi.org/10.1145/1935701.1935744`

44. Yuta Sugiura, Masahiko Inami, and Takeo Igarashi. 2012. A Thin Stretchable Interface for Tangential Force Measurement. In *Proceedings of the 25th Annual ACM Symposium on User Interface Software and Technology (UIST '12)*. ACM, New York, NY, USA, 529–536. `http://doi.org/10.1145/2380116.2380182`

45. Raw Material Suppliers. 2017. Print-On Silicone Ink. (2017). Retrieved April 1, 2017 from `http://rawmaterialsuppliers.com/print-on-silicone-rubber`.

46. Tyler N Tallman, Sila Gungor, K W Wang, and Charles E Bakis. 2015. Damage detection via electrical impedance tomography in glass fiber/epoxy laminates with carbon black filler. *Structural Health Monitoring* 14, 1 (2015), 100–109. `http://doi.org/10.1177/1475921714554142`

47. Karen Vanderloock, Vero Vanden Abeele, Johan A.K. Suykens, and Luc Geurts. 2013. The Skweezee System: Enabling the Design and the Programming of Squeeze Interactions. In *Proceedings of the 26th Annual ACM Symposium on User Interface Software and Technology (UIST '13)*. ACM, New York, NY, USA, 521–530. `http://doi.org/10.1145/2501988.2502033`

48. M Vauhkonen, W R B Lionheart, L M Heikkinen, P J Vauhkonen, and J P Kaipio. 2001. A MATLAB package for the EIDORS project to reconstruct two-dimensional EIT images. *Physiological Measurement* 22, 1 (2001), 107. `http://stacks.iop.org/0967-3334/22/i=1/a=314`

49. Wacker. 2017. ELASTOSIL LR 3162 A/B. (2017). Retrieved April 1, 2017 from `http://www.wacker.com`.

50. Martin Weigel, Tong Lu, Gilles Bailly, Antti Oulasvirta, Carmel Majidi, and Jürgen Steimle. 2015. iSkin: Flexible, Stretchable and Visually Customizable On-Body Touch Sensors for Mobile Computing. In *Proceedings of the 33rd Annual ACM Conference on Human Factors in Computing Systems (CHI '15)*. ACM, New York, NY, USA, 2991–3000. `http://doi.org/10.1145/2702123.2702391`

51. Michael Wessely, Theophanis Tsandilas, and Wendy E. Mackay. 2016. Stretchis: Fabricating Highly Stretchable User Interfaces. In *Proceedings of the 29th Annual Symposium on User Interface Software and Technology (UIST '16)*. ACM, New York, NY, USA, 697–704. `http://doi.org/10.1145/2984511.2984521`

52. Takeo Yamada, Yuhei Hayamizu, Yuki Yamamoto, Yoshiki Yomogida, Ali Izadi-Najafabadi, Don N. Futaba, and Kenji Hata. 2011. A stretchable carbon nanotube strain sensor for human-motion detection. *Nature Nano* 6, 5 (2011), 296–301. `http://doi.org/10.1038/nnano.2011.36`

53. K. Yamaguchi, J. J. C. Busfield, and A. G. Thomas. 2003. Electrical and mechanical behavior of filled elastomers. I. The effect of strain. *Journal of Polymer Science Part B: Polymer Physics* 41, 17 (2003), 2079–2089. `http://doi.org/10.1002/polb.10571`

54. Lining Yao, Ryuma Niiyama, Jifei Ou, Sean Follmer, Clark Della Silva, and Hiroshi Ishii. 2013. PneUI: Pneumatically Actuated Soft Composite Materials for Shape Changing Interfaces. In *Proceedings of the 26th Annual ACM Symposium on User Interface Software and Technology (UIST '13)*. ACM, New York, NY, USA, 13–22. `http://doi.org/10.1145/2501988.2502037`

55. Sang Ho Yoon, Ke Huo, Vinh P. Nguyen, and Karthik Ramani. 2015. TIMMi: Finger-worn Textile Input Device with Multimodal Sensing in Mobile Interaction. In *Proceedings of the Ninth International Conference on Tangible, Embedded, and Embodied Interaction (TEI '15)*. ACM, New York, NY, USA, 269–272. `http://doi.org/10.1145/2677199.2680560`

56. Sang Ho Yoon, Yunbo Zhang, Ke Huo, and Karthik Ramani. 2016. TRing: Instant and Customizable Interactions with Objects Using an Embedded Magnet and a Finger-Worn Device. In *Proceedings of the 29th Annual Symposium on User Interface Software and Technology (UIST '16)*. ACM, New York, NY, USA, 169–181. `http://doi.org/10.1145/2984511.2984529`

57. Yang Zhang, Gierad Laput, and Chris Harrison. 2017. Electrick: Low-Cost Touch Sensing Using Electric Field Tomography. In *Proceedings of the 2017 CHI Conference on Human Factors in Computing Systems (CHI '17)*. ACM, New York, NY, USA, 1–14. `http://doi.org/10.1145/3025453.3025842`

58. Yang Zhang, Robert Xiao, and Chris Harrison. 2016. Advancing Hand Gesture Recognition with High Resolution Electrical Impedance Tomography. In *Proceedings of the 29th Annual Symposium on User Interface Software and Technology (UIST '16)*. ACM, New York, NY, USA, 843–850. `http://doi.org/10.1145/2984511.2984574`